Chemistry Europe
European Chemical Societies Publishing

Special Collection

Circularly Polarized Fluorescent Helicene-Boranils: Synthesis, Photophysical and Chiroptical Properties

Aurélie Macé,[a] Khaoula Hamrouni,[a, b] Etienne S. Gauthier,[a] Marion Jean,[c] Nicolas Vanthuyne,[c] Lucas Frédéric,[d] Grégory Pieters,[d] Elsa Caytan,[a] Thierry Roisnel,[a] Faouzi Aloui,[b] Monika Srebro-Hooper,*[e] Bertrand Carboni,[a] Fabienne Berrée,*[a] and Jeanne Crassous*[a]

In memory of François Diederich

Abstract: Mono- and di-boranil-substituted helicenes were prepared by BF_2-borylation of the corresponding anils, readily synthesized by condensation of 2-amino- and 2,15-diamino-helicenes with 4-(diethylamino)salicylaldehyde. After enantiomeric resolution using HPLC, their chiroptical properties including circularly polarized fluorescence in solution and in PMMA films were investigated and rationalized with the help of NMR, X-ray and quantum-chemical calculations.

Introduction

Helicenes are chiral, screw-like shaped, polyaromatic hydrocarbons (PAHs) displaying strong chiroptical activity.[1] Recently, a particular focus has been put on their circularly polarized emission (CPL)[2] for future potential applications in cryptography, circularly polarized organic light-emitting diodes (CP-OLEDs) technology, bioimaging or photocatalysis.[3] At the molecular level, chiral organic molecules display CPL activity with luminescence dissymmetry factors ($g_{lum} = 2(I_L - I_R)/(I_L + I_R)$) of 10^{-4}–10^{-2}, due to underlying electric dipole-allowed electronic transitions, resulting in not necessarily small $I_L - I_R$, but quite large $I_L + I_R$, thus diminishing g_{lum} values. Despite this, such systems have emerged as valuable candidates for CPL applications thanks to their tunable photophysical properties along with easy processing and integration into optoelectronic devices.[3] In comparison, chiral lanthanide complexes are known to show g_{lum} values that can reach more than 1 thanks to their f→f electronic transitions, formally forbidden by Laporte selection rules, which lead to very small $I_L + I_R$.[4] However, emission quantum yields reported for such compounds are usually low.

Among all the CPL-active organic small molecules, helicenes have been shown to display rather strong CPL activity with g_{lum} values as high as 10^{-2}.[5] Recently, the possibility to incorporate heteroatoms (Si, S, B, N, P) into helicene frameworks using various synthetic strategies has attracted a special attention with the aim of creating/expanding structural diversity and tuning the photophysical properties of such systems.[6] In this regard, incorporating boron atoms into helicenes can be considered as a valuable strategy to generate novel chiral materials with tailored properties. For instance, due to the electron-accepting and Lewis acidic characters of boron, introducing one or several B atoms into a helicenic scaffold generally results in strongly blue-emitting chiral fluorophores, such as in CPL-active azaborahelicenes **H1**#[7] and **H2**#[8] (Figure 1). The three- or four-coordinate nature of the boron atom enables to construct not only monohelicenic, but also multi-helicenic units, such as oxabora-bishelicenic system **H3**#.[9] BF_2 fragments can also be introduced within azahelicene units and yield efficient CPL-active orange or red emitters, such as **H4**#[10a] or **H5**#,[11] thus showing that the luminescence can be readily tuned by choosing appropriate boron-doped chromophore. The CPL emission can be further modulated by post-functionalizing the same chiral system with, for instance, a chiral binaphthol substituent on the boron atom in place of the two fluorines.[10b] Finally, instead of incorporating aza- or oxa-boracycles into the fused helicenic scaffold, boron-based fragments can be grafted onto a helical core, as shown in the configurationally stable

[a] *Dr. A. Macé, K. Hamrouni, Dr. E. S. Gauthier, Dr. E. Caytan, Dr. T. Roisnel, Dr. B. Carboni, Dr. F. Berrée, Dr. J. Crassous*
Univ Rennes, CNRS, ISCR-UMR 6226
Université de Rennes 1, Campus de Beaulieu, 35042 Rennes Cedex (France)
E-mail: fabienne.berree@univ-rennes1.fr
jeanne.crassous@univ-rennes1.fr

[b] *K. Hamrouni, Dr. F. Aloui*
University of Monastir, Faculty of Sciences, Laboratory of Asymmetric Synthesis and Molecular Engineering of Materials for Organic Electronics (LR18ES19), Avenue of Environment 5019 Monastir (Tunisia)

[c] *M. Jean, Dr. N. Vanthuyne*
Aix Marseille University, CNRS, Centrale Marseille, iSm2, Marseille (France)

[d] *Dr. L. Frédéric, Dr. G. Pieters*
Université Paris-Saclay, CEA, Département Médicaments et Technologies pour la Santé (DMTS), SCBM, Gif-sur-Yvette, 91191 (France)

[e] *Dr. M. Srebro-Hooper*
Faculty of Chemistry, Jagiellonian University
Gronostajowa 2, 30-387 Krakow (Poland)
E-mail: srebro@chemia.uj.edu.pl

Supporting information for this article is available on the WWW under https://doi.org/10.1002/chem.202100356

Special Collection *This article belongs to a Joint Special Collection dedicated to François Diederich.*

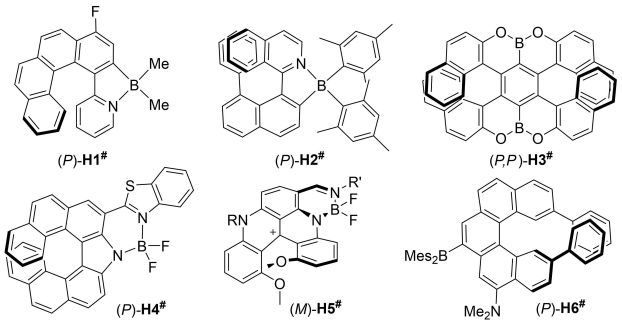

Figure 1. Chemical structures of known boron-based helicene derivatives.

pentahelicenic structure **H6**#, which is functionalized with a $BMes_2$ moiety (Mes = mesityl).[12] In this system, the presence of electron-donating NMe_2 unit allowed to tune the emission to more red-shifted wavelengths thanks to a strong charge transfer. Furthermore, the vacant p_z orbital of boron enabled to use **H6**# as a fluoride anion sensor with CPL signal as a read-out response. Note that along with the boron atom, N or O atoms are often introduced *via* B–N or B–O bonds. Indeed, the interaction between the N/O lone pair and the unoccupied p_z B orbital enhances the chemical stability of such molecules. Otherwise, sterically hindered substituents, such as mesityls in **H6**#, need to be introduced to protect the boron atom.

Boranils, another class of boron heterocycles derived from salicylaldanilinimines, possess an N–B–O connectivity and are particularly promising species due to their attractive optical features.[13] Following the pioneering work of Hohaus et al. in 1973,[14] Ulrich, Ziessel et al. reported in 2011 the facile two-steps preparation of boranils bearing donor/acceptor substituents, showing higher stability compared to their unsubstituted congeners and good luminescence properties in solution and solid states.[15] In addition, such compounds have the major advantage of being easily synthesized, even on a large-scale, from a variety of anilines or amines, including chiral ones. Although a few chiral boranils[16] or related BF_2 compounds[17] with salicylaldehyde-based Schiff-base *N^O*-containing ligands have been addressed so far, only few of them are CPL-active.

Herein, we report the preparation and detailed characterization of novel boron-containing helicenes **H1**-**H3**, which combine carbo[4]- or carbo[6]-helicene moieties and one or two boranil units (Figure 2). In particular, the chiroptical properties of enantiopures **H2** and **H3**, together with their nonpolarized and circularly polarized fluorescence, were examined and rationalized with the help of first-principles calculations.

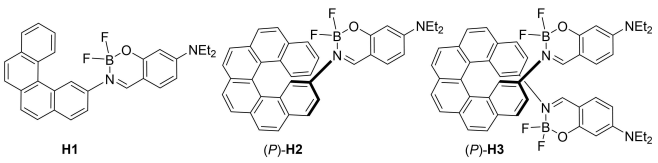

Figure 2. Chemical structures of new helicene-boranils presented in this work.

Results and Discussion

Synthesis and structural characterization of helicene-boranils H1-H3

Helicene-boranils **H1**-**H2** were first prepared following the general synthetic route depicted in Scheme 1. Namely, helicene-boronate derivatives **1a**–**b** were first converted into helicene-amines **2a**–**b**,[18] which, in turn, gave imines **3a**–**b** by treatment with 4-(diethylamino)salicylaldehyde. A final complexation with $BF_3{\cdot}OEt_2$ in the presence of *N*,*N*-diisopropylethylamine (DIEA), in refluxing 1,2-dichloroethane (1,2-DCE) for 24–42 hours yielded the targeted compounds.

Following the same approach, [6]helicene-2,15-bis-pinacolboronate **1c** was first prepared according to Scheme 2, *i.e.* in

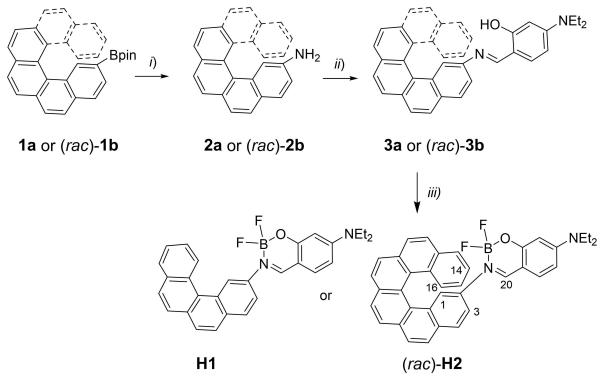

Scheme 1. Synthesis of helicene-boranils **H1**-**H2** from helicene-boronates **1a**–**1b**. *i*) NaN_3, $CuSO_4{\cdot}5H_2O$, MeOH, reflux, 19 hrs, then H_2, 10% Pd/C, EtOAc rt, 24 hrs, **2a**: 65%, **2b**: 75%; *ii*) 4-(diethylamino)salicylaldehyde, MeOH, reflux, **3a**: 18 hrs, 91%, **3b**: 31 hrs, 93%; *iii*) $BF_3{\cdot}OEt_2$, DIEA, 1,2-DCE, 85 °C, **H1**: 42 hrs, 75%, (*rac*)-**H2**: 24 hrs, 75%.

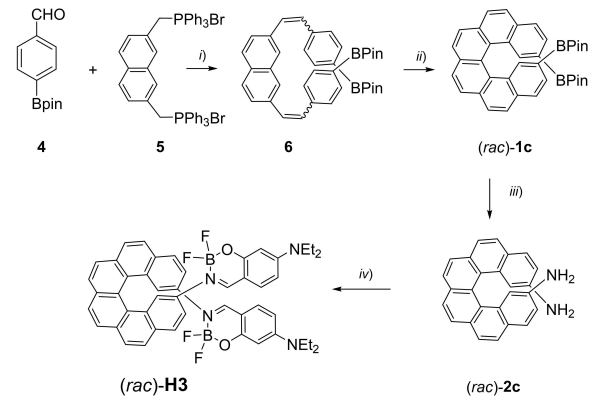

Scheme 2. Synthesis of racemic boranil **H3**. *i*) *n*-BuLi, THF, Ar, rt, 3 hrs, 58%; *ii*) *hν*, I_2, propylene oxide, toluene, Ar, 18 hrs, 57%; *iii*) NaN_3, $CuSO_4{\cdot}5H_2O$, MeOH, 40 °C, 27 hrs, then H_2, 10% Pd/C, EtOAc rt, 24 hrs, 67%; *iv*) 4-(diethylamino)salicylaldehyde, MeOH, reflux, 22 hrs, 98%, then $BF_3{\cdot}OEt_2$, DIEA, 1,2-DCE, 85 °C, 23 hrs, 91%.

two steps involving a Wittig reaction between 4-formylphenylboronic acid pinacol ester **4** and (2,7-naphthalenedimethylene)-bis[triphenylphosphonium-bromide][19a] **5** (58% yield based on recovered phosphonium salt, see Supporting Information), followed by an oxidative photocyclization reaction. Note that **1c** has also been recently synthesized using another strategy from 2,15-bis-bromo-carbo[6]helicene.[19b] The helicenic aniline **2c** was then prepared in a 67% overall yield by copper-catalyzed azidation using copper sulfate in refluxing methanol and hydrogenation with H_2 in the presence of Pd/C. Refluxing **2c** with 4-(diethylamino)salicylaldehyde in methanol for 22 hours afforded the anil, which was converted to **H3** (91% yield) as previously described for **3a**–**b**.

The resulting novel helicenic boranils **H1**-**H3** were then fully characterized by NMR and mass spectrometry (see Supporting Information). While the ^{1}H and ^{13}C NMR spectra display the typical, characteristic signals coming from both the helicene and boranil units, these compounds show very informative ^{11}B NMR and ^{19}F NMR (see Table 1 and Supporting Information). Indeed, **H1** displays two chemically and magnetically equivalent fluorine atoms that resonate at −136.5 ppm and demonstrate similar B–F coupling constants ($^{1}J_{B-F}$ = 17.3 Hz). The ^{11}B NMR spectra show a triplet at δ = 1.1 ppm in agreement with a four-coordinate boron atom. By contrast, chiral **H2** displays two distinct ^{19}F NMR signals that are doublets of 1:1:1:1 quadruplets, at −129.7 (dq, $^{2}J_{F-F}$ = 90 Hz, $^{1}J_{B-F}$ = 23 Hz) and −143.4 ppm ($^{2}J_{F-F}$ = 90 Hz, $^{1}J_{B-F}$ = 11.1 Hz). The corresponding ^{11}B NMR signal demonstrates a doublet of doublets (dd) at 0.6 ppm with different coupling constants with the two fluorine atoms. Carbo[6]helicene-2,15-bis-boranil **H3** displays very similar features, *i.e.* dq signals for each fluorine and dd for the boron, with the two BF_2 groups being equivalent indicating C_2-symmetry of the molecule.[20]

Enantiomeric resolution of (*rac*)-**H2** and (*rac*)-**H3** was performed using HPLC over chiral stationary phases, yielding (*P*)-(+) and (*M*)-(−) enantiomers of **H2** and **H3** with *ee* values higher than 99% (see Supporting Information). Single crystals of (+)-**H2** were grown by slow diffusion of pentane vapors into a CH_2Cl_2 solution and the structure was further ascertained by X-ray diffraction crystallography. Compound (+)-**H2** crystallized in the non-centro-symmetric $P2_12_12_1$ space group (with the presence of *P* enantiomers only, see Figures 3a,b). The molecular structure shows a C_1 symmetry with a helicity (dihedral angle between terminal rings of the helicene) of 52.34°, a typical value for a carbo[6]helicene.[1] The O–B and the B–N_1 bond-lengths are 1.445 and 1.582 Å, respectively, which are in the range of similar 4-coordinate boron(III) derivatives. Interestingly, the helicenic and the boranil parts are linked through a C–N single bond (with a length of 1.433 Å), which displays axial chirality due to a B–N_1–C–C′ dihedral angle of −50.51°, thus representing the (R_a) configuration associated with the (*P*) stereochemistry of the carbo[6]helicene fragment. There is therefore an interesting chiral induction from the helicenic part

Table 1. ^{11}B and ^{19}F NMR data recorded in $CDCl_3$ at rt for compounds **H1**-**H3**. See also Supporting Information.

Compound	^{11}B δ (ppm) (multiplicity)	J_{B-F} (Hz)	^{19}F δ (ppm) (multiplicity)	J_{F-F} (Hz)
H1	1.1 (t)	17.3	−136.5 (q)	–
H2	0.6 (dd)	23.0 and 11.1	−129.7 (dq) and −143.4 (dq)	90
H3	0.5 (dd)	22.7 and 10.3	−129.7 (dq) and −142.7 (dq)	89.8

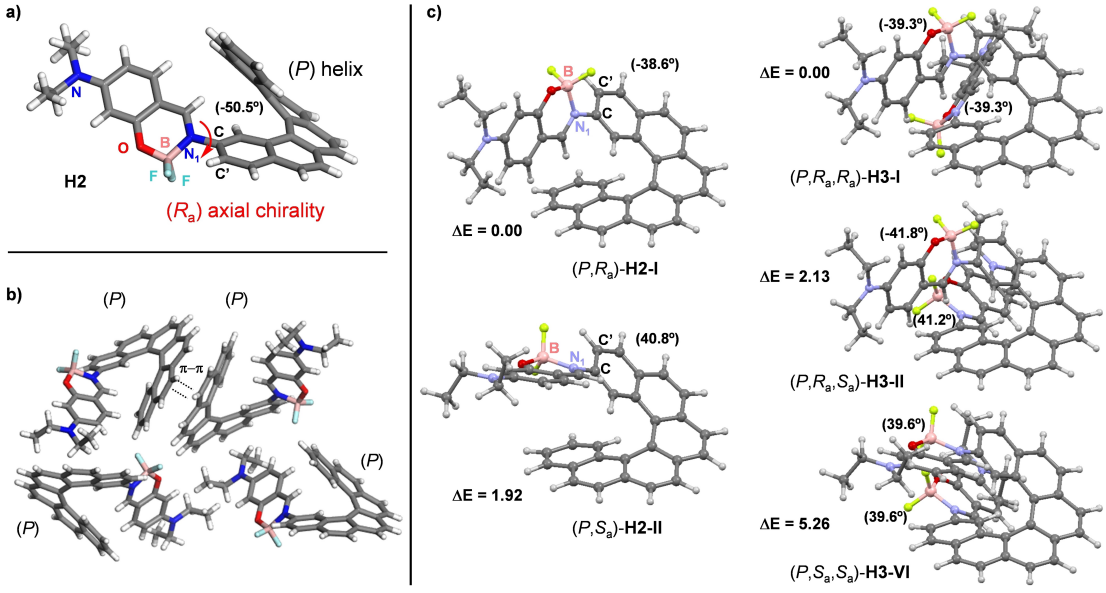

Figure 3. a) X-ray diffraction structure of (*P*)-(+)-**H2** with (R_a) axial chirality highlighted along with b) its supramolecular arrangement in the crystal. c) Selected optimized (BP/SV(P) with the continuum solvent model for CH_2Cl_2) structures of **H2** (left) and **H3** (right). Compare with Table 2 and see Supporting Information for a full set of data. Values listed are the corresponding relative energies ΔE (in kcal/mol) calculated with BP-D3/TZVP and the B–N_1–C–C′ dihedral angles (provided in parentheses). Deposition number 2047289 contains the supplementary crystallographic data for this paper. These data are provided free of charge by the joint Cambridge Crystallographic Data Centre and Fachinformationszentrum Karlsruhe Access Structures service.

to the axial chirality in the solid state. This can be explained by the position of the more sterically hindered BF_2 group away from the helix and the existence of a CH-π interaction between the proton of the CH=N imine and the external terminal ring of the carbo[6]helicene (Figure 3a, H-centroid distance: 2.771 Å) that 'locks' the structure into a closed form in the crystal. Finally, intermolecular π-π stacking interactions (Figure 3b) are observed in the molecular packing of homochiral dimers. Note that the molecular geometry of **H2** observed in its crystal structure may not necessarily be dominant in solution, as a careful analysis of the NOESY spectrum of this compound showed that the proton H^{20} (of the CH=N imine) correlates with H^{13} and H^{14} (other extremity of the helicene) and with both H^1 and H^3 (see Figures S1.16a–b), thus suggesting the fast rotation around the C^2–N (C–N_1 in Figure 3a) bound (in the NMR timescale). Similar conclusion holds also for **H3**, for which the analogous correlation of protons in the NOESY spectrum is seen (H^{12} with H^1, H^3 and H^4, see Figures S1.37a–b).

Stereochemical and structural preferences for helicene-boranils **H1**, **H2**, and **H3** in solution were also examined with quantum-chemical calculations. DFT geometry optimizations (BP/SV(P) with the continuum solvent model for CH_2Cl_2, followed by BP-D3/TZVP electronic energy evaluation; for a complete description of the computational details, see Supporting Information) considered different possible diastereoisomers (based on (*P*) helical stereochemistry associated with either (R_a) or (S_a) axial conformational chirality) with different rotamers for the relative orientation of the boranil fragment(s) and the helicene. The results (see Figure 3c and Table 2, and Figures S2.2-S2.3 and Table S2.1 in SI) show profound energetic preferences for the **H2** and **H3** structures demonstrating a combination of the (*P*) and (R_a) configurations stabilized by the intramolecular CH-π boranil-helicene interaction, labelled in the following as (*P*,R_a)-**H2-I** and (*P*,R_a,R_a)-**H3-I**. Coexistence of other diastereoisomeric structures in solution mixture, such as for example (*P*,S_a)-**H2-II** or (of mixed axial chirality) (*P*,R_a,S_a)-**H3-II**, is however quite likely as their energy values were found to be relatively close to those computed for the corresponding structures I. An energetic barrier for a rotation around the boranil-helicene bond is expected to be low, resulting in the overall high molecular flexibility of the systems. All this correctly reflects the results of the experimental (X-ray diffraction crystallography and NMR) studies presented above. For the [4]helicene-boranil **H1** a roughly equal mixture of possible diastereoisomers is expected based on the calculated data (see Supporting Information).

Table 2. Summary of computed (BP/SV(P) with the continuum solvent model for CH_2Cl_2) rotamer structures for helicene-boranils **H2** and **H3**: B–N_1–C–C′ dihedral angles as defined in Figure 3 (∠, in °) along with relative energies (Δ*E*, in kcal/mol) calculated with BP-D3/TZVP and the corresponding Boltzmann populations at 25 °C (n_B, in %). For structures visualization, see Figure 3 and Supporting Information.

Structure		∠	Δ*E*	n_B
P-**H2**	(*P*,R_a)-I	−38.64	0.00	94.6
	(*P*,S_a)-II	40.84	1.92	3.7
	(*P*,R_a)-III	−136.69	2.40	1.6
	(*P*,S_a)-IV	136.75	3.94	0.1
P-**H3**	(*P*,R_a,R_a)-I	−39.34/−39.34	0.00	93.2
	(*P*,R_a,S_a)-II	−41.83/41.23	2.13	2.6
	(*P*,S_a,R_a)-III	42.70/−131.51	2.20	2.2
	(*P*,R_a,R_a)-IV	−38.01/−136.01	2.28	2.0
	(*P*,R_a,R_a)-V	−136.88/−136.88	4.83	0.0
	(*P*,S_a,S_a)-VI	39.59/39.59	5.26	0.0
	(*P*,S_a,S_a)-VII	138.20/142.38	7.14	0.0

Photophysical properties: UV-vis spectroscopy

The UV-vis spectra of the [*n*]helicene-boranils **H1**-**H3** were measured in CH_2Cl_2 solution at concentrations *ca.* 10^{-5} M and they are presented in Figure 4a. The [4]helicene-boranil **H1** system displays two main wide and strong bands comprising: *i*) two signals at 270 and 284 nm ($\varepsilon \sim 30000$; please note that all ε in this work are given in units of $M^{-1}cm^{-1}$) accompanied with broad structuration and *ii*) an even stronger signal at 415 nm ($\varepsilon \sim 38000$). Reflecting an increase in the π-electron system, the [6]helicene-mono-boranil **H2** and bis-boranil **H3** exhibit stronger UV-vis responses as compared to **H1**, with three main sets of bands that include: *i*) a set of two signals at 246 and 255 nm ($\varepsilon \sim 53000$) for **H2**, which are weaker in **H3** (243–255 nm, $\varepsilon \sim 33000$), *ii*) a set of three signals at 305, 333 and 351 nm ($\varepsilon =$ 22000–29100) for **H2**, which appear at 305, 343 and 356 nm ($\varepsilon =$ 19000–27500) for **H3**, and *iii*) a strong signal at 409 nm ($\varepsilon =$ 50000) with shoulders at 390 and 423 nm for **H2** that corresponds to a strongly enhanced one at 412 nm ($\varepsilon = 70000$) with shoulders at 393 and 433 nm for **H3**.

To shed some light on the electronic origin of these bands, time-dependent DFT (TD-DFT) calculations were then performed. See Supporting Information for all computational details and a full set of computed data. The simulated UV-vis spectra of **H1**, **H2**, and **H3** do not differ much for different diastereomeric structures and visibly fail to reproduce experimental relative intensities of the lowest-energy band for **H1** *vs.* **H2**-**H3** (overestimating the intensity for **H1**) and of the two bands around 330 nm and 410 nm for **H2** and **H3** (overestimating the intensity for the higher-energy – shorter-wavelength – band); see the discussion below. However, other important spectral features observed in the experiments (such as relative and absolute energetic positions of the bands along with a substantial increase in the low-energy absorption intensity when going from **H2** to **H3**) appear to be overall well-described by theory (PBE0/SV(P) with a continuum solvent model for CH_2Cl_2, see Figure S2.7), enabling assignment of the particular bands. Namely, analysis of molecular orbital (MO) pair contributions to selected excitations for **H1**, **H2**, and **H3** shows that the high-energy intense band of these systems observed experimentally around 275 nm for **H1** and 250 nm for **H2** and **H3** originates from predominatly helicene-centered π-π* excitations with contributions from helicene→boranil and boranil→helicene charge-transfer (CT) transitions. The UV-vis intensity around 330 nm can be, on the other hand, assigned to a combination of mainly boranil→helicene and helicene→boranil CTs mixed with π–π* transitions within helicene fragment. Such assignments account for strong enhancement in absorption observed experimentally in this spectral range for

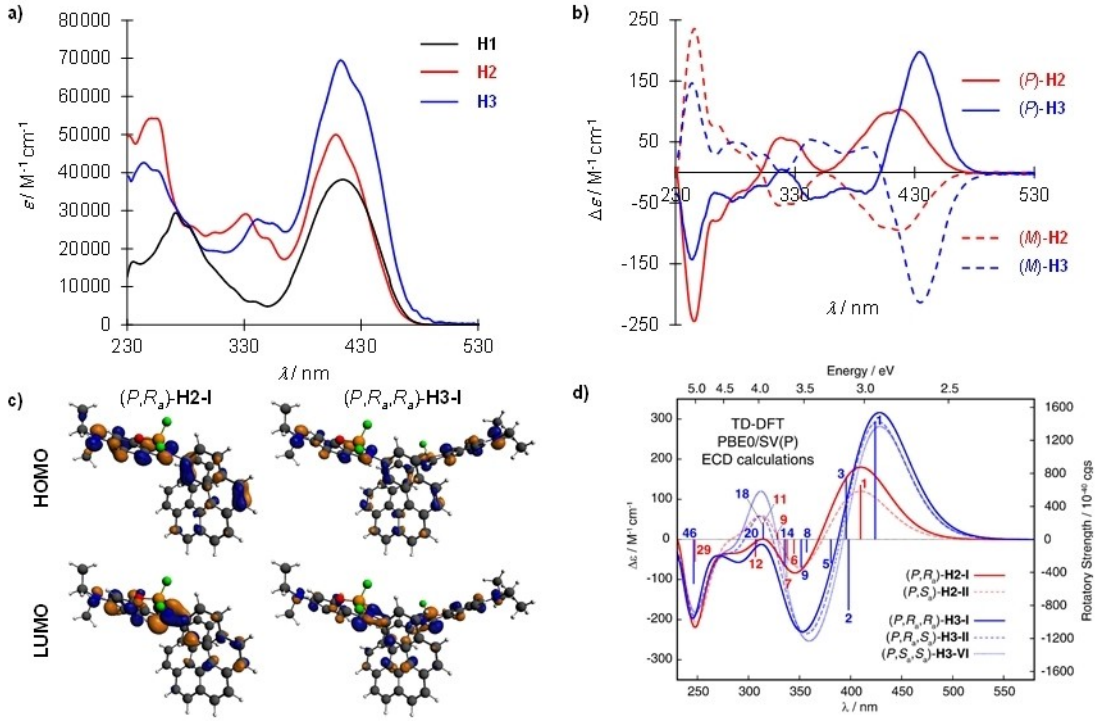

Figure 4. Experimental a) UV-vis of **H1**-**H3** and b) ECD spectra of (*P*) and (*M*) enantiomers of **H2** and **H3** (CH_2Cl_2, $C \sim 10^{-5}$ M). c) Isosurfaces (±0.04 au) of frontier MOs of the lowest-energy computed **H2** and **H3** structures. d) Simulated ECD spectra for representative (*P*) diastereoisomers of **H2** and **H3** with selected calculated excitation energies and rotatory strengths (for structures I) indicated as "stick" spectra. See Supporting Information for a full set of data.

the more π-extended [6]helicene-based **H2** and **H3** compared to the [4]helicene derivative **H1**. Finally, the computations indicate that the lowest-energy band of all three systems, centered around 410 nm, is due to excitations involving highest occupied (HO) and lowest unoccupied (LU) MOs (HOMO/LUMO for **H1**, **H2**; HOMO-1, HOMO/LUMO, LUMO + 1 for **H3**; see Figure 4c and Supporting Information) and accordingly corresponding to π-π* transitions within the boranil fragment(s) π-conjugated with the adjacent helicene rings. As the orbitals are centered in slightly different parts of the π-electron system, the excitations demonstrate also some CT signature.

Note that HOMO-1, HOMO, LUMO, and LUMO + 1 of **H3** have electronic density extended over both boranil substituents and partially also over the helicene, but in-phase and out-of-phase linear combinations may be taken where electronic density localizes on one boranil (and adjacent helicene rings) fragment. While in the case of **H1** and **H2**, one intense excitation contributes to this band (no. 1 calculated at respectively *ca.* 400 nm and 410 nm), for **H3** an intense pair of excitations was computed in this spectral region (no. 1 at *ca.* 420 nm and no. 2 at *ca.* 400 nm) that may indicate exciton coupling between the two boranil-helicene π–π* transitions, similar to what we previously showed for push-pull helicenic diketopyrrolopyrrole systems.[21a] This can rationalize a red-shift of the lowest-energy absorption band and an increase in its intensity observed experimentally for **H3** as compared to **H2**.

Chiroptical properties: Electronic circular dichroism, optical rotation

The electronic circular dichroism (ECD) spectra and optical rotation (OR) values of the [6]helicenic derivatives **H2** and **H3** were also examined (Figure 4, Table S1.1, Supporting Information; please note that all $\Delta\varepsilon$ in this work are given in units of $M^{-1}\,cm^{-1}$, while specific rotations are given in degree $[dm\,g\,cm^{-3}]^{-1}$). Both systems display strong specific rotation values ($[\alpha]_D^{25} = +3900$ and $+3550$ for (*P*)-**H2** and (*P*)-**H3**, respectively) that are similar to other carbo[6]helicenes.[1] As depicted in Figure 4b, the (*M*) and (*P*) enantiomers display the expected mirror-image ECD spectra. The three sets of bands observed in UV-vis spectra are ECD-active in both **H2** and **H3**. For instance, (*P*)-**H2** displays: *i*) a strong negative band at 245 nm ($\Delta\varepsilon = -244$) accompanied with two weaker ones at 265 (−79) and 290 nm (−29), *ii*) two positive bands of moderate intensity at 319 (+57) and 329 nm (+51), and *iii*) two strong positive bands at 407 (+98) and 417 nm (+103). Overall the ECD spectral envelope of this [6]helicene-based system is strikingly different from those measured for the classical helicenic compounds such as nonsubstituted carbo[*n*]helicenes.[1] This is also the case for the helicene-bis-boranil **H3**, whose (*P*) enantiomer exhibits overall the same characteristic bands in its ECD spectrum as (*P*)-**H2**, but with different relative intensities or signs and a clear red-shift of the lower-energy bands, *i.e. i*) a weaker negative band at 244 (−143) accompanied with other ones at 277 (−48), 284 (−41), and 307 nm

(−11), *ii*) three negative bands of moderate intensity at 343 (−44), 355 (−39) and 389 nm (−35), and *iii*) one strong positive band at 435 nm (+197).

The TD-DFT-simulated[22] (PBE0/SV(P) with a continuum solvent model for CH_2Cl_2) ECD spectra for selected **H2** and **H3** diastereomeric structures are presented in Figure 4d; see also Supporting Information for additional calculated data. ECD spectral envelope obtained for the energetically most preferred conformer (P,R_a)-**H2-I**, as indicated by DFT, (see Figure 3c and Table 2), resembles the experimental ones but with "too negative" intensity between *ca.* 375 and 300 nm. The corresponding (P,S_a)-**H2-II** structure (of relatively low energy) demonstrates very similar ECD spectrum but with a decreased intensity of the first low-energy positive band and, more importantly, with appearance of a positive band of moderate intensity around 325 nm that matches well the second positive band observed for this compound in the experiment. It is worth mentioning that the spectral data obtained for other optimized **H2** geometries clearly confirm a high sensitivity of the ECD intensity in the low- and medium-energy range to the rotamer structure and particularly to its axial chirality (see Figure S2.4 and Figure 4d), with the (P,S_a) diastereoisomers emerging as predominantly responsible for the positive ECD signal measured at *ca.* 325 nm. This further supports the coexistence of various **H2** structures of both (R_a) and (S_a) axial chirality in solution mixture also suggested based on the NMR studies (*vide supra*). An analysis of the dominant excitations of the simulated spectra of (P,R_a)-**H2-I** and (P,S_a)-**H2-II** conformers assigns the intense negative ECD band centered at *ca.* 250 nm to excitations involving predominantly, as expected, π-π* transitions within the helicene moiety (*e.g.* excitation no. 29 calculated at 247 nm), although with additional small CT contributions mostly of the boranil→helicene origin. The lowest-energy positive band measured around 410 nm corresponds to the HOMO-to-LUMO π–π* transitions centered mainly at the boranil chromophore with noticeable involvement of helicene π-orbitals electronically coupled with the boranil π-electron system (excitation no. 1 calculated at *ca.* 410 nm). The decrease in positive ECD intensity experimentally observed at around 350 nm for the (*P*)-**H2** enantiomer appears to originate from excitations representing a combination of predominantly boranil→helicene CTs and helicene-centered π–π* transitions of CT-like signature mixed with additional small contributions from helicene→boranil CTs and π–π* transitions within the boranil fragment (*e.g.* excitations nos. 6 and 7 calculated at *ca.* 345 and 336 nm, respectively). The overestimation of this intensity drop observed in the computations (leading to the appearance of the negative band in the calculated spectra) is likely due to neglecting vibrational effects and/or disregarding contributions from other less-energetic (equilibrium) conformers. In the former matter, not only vibronic contributions (note that indeed both UV-vis and ECD experimental spectra for all the systems studied show vibronic fine structure),[23] but also nonequilibrium structure effects,[24] might be crucial here to ensure a satisfactory agreement of the simulated spectra with experiments. In particular, we speculate that vibrational bending of the boranil-helicene bond can reduce/break the electronic π-conjugation between both fragments that is expected to affect intensity of excitations within these systems.[25] This is indeed supported by a substantial modification of the ECD intensity found for some BP-D3-optimized structures in which the boranil moiety strongly (and likely exaggeratedly) bent towards terminal rings of the helicene (see Supporting Information). Finally, the ECD signal around 325 nm appears to be due to several excitations of sizable calculated rotatory strengths (R) differing in sign that demonstrate mainly a mixed helicene-/boranil-centered π-π* and helicene→boranil/boranil→helicene CT character (*e.g.* excitations nos. 9 (+), 11 (+), and 12 (−) calculated at *ca.* 328, 314, and 307 nm, respectively); magnitudes of R for these excitations are clearly dependent on a molecular structure leading to a cancellation of their ECD intensity in the simulated spectrum for (P,R_a)-**H2-I** or an appearance of a positive intensity in the case of, for example, (P,S_a)-**H2-II**.

As can be seen in Figure 4, the simulated ECD spectrum for the calculated lowest-energy structure (P,R_a,R_a)-**H3-I** (see Figure 3c and Table 2), agrees quite well with the experimental data. In particular, it correctly reproduces a red-shift and increase in intensity of the lowest-energy positive band along with appearance of more negative intensity between *ca.* 400 and 280 nm that were observed in the experimental ECD spectra of (*P*)-**H3** *vs.* (*P*)-**H2**. Similarly to the mono-boranil **H2**, a visible dependence of the bands intensity in the simulated ECD spectra on the molecular structure of **H3** was also noted, with (S_a) axial chirality giving its clear signature in form of a positive band centered around 325 nm (see Figure S2.5 and Figure 4d). Since in the experiment a weakly intense positive band was indeed observed in this spectral region, coexistence of various structures of both (R_a) and (S_a) configurations in solution might also be postulated for **H3**. The assignment of the **H3** ECD spectrum is qualitatively similar to that of **H2**. Namely, predominantly boranil- and helicene-centered π–π* transitions were found to be responsible for respectively lowest-energy positive (*ca.* 430 nm) and highest-energy negative (*ca.* 240 nm) bands present in the experimental spectrum (see excitations nos. 1 and 46 calculated at *ca.* 420 nm and 245 nm), while the negative ECD intensity appearing between *ca.* 400 and 280 nm origin from helicene→boranil and boranil→helicene CT excitations mixed with π-π* transitions within boranils and helicene fragments (see *e.g.* excitations nos. 5, 8, 9, and 14 calculated between around 380 and 330 nm). These latter excitations, demonstrating sizable negative rotatory strength values, enhanced compared to **H2** reflecting the presence of the second boranil chromophore, lead to a very intense negative band in the simulated spectrum that is strongly overestimated compared with the experimental one likely due to similar reasons as for **H2** (*vide supra*). As in the case of **H2**, a sign of ECD intensity around 325 nm for **H3** appears to stem from a cancellation ((P,R_a,R_a)-**H3-I**) or enhancement ((P,R_a,S_a)-**H3-II** and (P,S_a,S_a)-**H3-VI**) of intensity of the underlying excitations representing a combination of mainly boranil- and helicene-centered π–π* transitions.

Despite the similarities between the mono-boranil **H2** and bis-boranil **H3** systems, a striking difference can be noted in

their low-energy ECD-active excitations. Namely, unlike for (*P*)-**H2**, for which calculations showed one intense excitation underlying the lowest-energy band in the spectrum (excitation no. 1 computed at *ca.* 410 nm, *vide supra*), in the case of (*P*)-**H3** an intense pair of excitations involving HOMO-1, HOMO, LUMO, and LUMO+1 is present in this spectral region (excitations nos. 1 and 2 at around 420 and 400 nm, respectively) that both reveal the same (and shared with **H2**) predominantly boranil-centered π-π* character with a noticeable involvement of the helicene π-orbitals but demonstrate opposite-sign rotatory strengths ((+) and (−) for the lower-energy and higher-energy excitation, respectively). The electronic and MO-pair assignment, large rotatory strengths and the opposite signs of these first two excitations clearly indicate exciton coupling between the electric transition dipoles of the boranil fragments grafted onto the extremities of **H3**, with noticeable contributions from the helicene π-system, similar to what was shown by us recently for helicene-diketopyrrolopyrrole derivatives.[21a] It should be however noted that unlike for the helicene-diketopyrrolopyrrole systems, in the case of (*P*)-**H3** higher-energy negative exciton couplet component does not appear to contribute much to the following negative band in the ECD spectrum as it seems to be efficiently suppressed by the nearby excitation with large positive rotatory strength value (excitation no. 3 calculated at *ca.* 395 nm) corresponding to boranil-centered π–π* transition mixed with helicene→boranil CT.

Luminescence properties

Boranil derivatives can display appealing emission properties, notably also in the solid state, and may show Aggregation-Induced Emission (AIE) or Aggregation-Induced Emission Enhancement (AIEE) effects.[16,17,26] The luminescence properties of compounds **H1**-**H3** were thus recorded in CH_2Cl_2 at room temperature (rt, 298 K) and in the solid state. The rt emission spectrum of **H1** is displayed in Figure S1.43, showing two fluorescence signals, at 480 and 504 nm; a quantum yield of 4% (λ_{exc} = 350 nm) was measured. The [6]helicene derivatives **H2** and **H3** also display two main fluorescence signals, at respectively 485–515 nm (Figure 5a) and 493–520 nm (Figure 5b), thus only slightly red-shifted compared to **H1**, but with visibly enhanced quantum yields of 30% and 20%; these values are quite high for [6]helicenes[1] and consistent with the results for other boron derivatives.[9–12,16,17] Note that the emission spectra were also measured in other solvents but no solvatochromism was observed. Finally, the luminescence properties of **H2** and **H3** were examined in powders and quantum yields were found to be 8% at 519 nm for the mono-boranil and almost zero for the bis-boranil derivative. Note that AIE enhancement was studied in water/THF mixtures but no effect was observed for these systems.

Similar luminescence properties of **H1**-**H3** along with the similarity of their corresponding lowest-energy absorption may indicate fundamentally identical nature of the emitting S_1 state for all three systems. This was indeed ascertained using TD-DFT calculations (PBE0/SV(P) with a continuum solvent model for

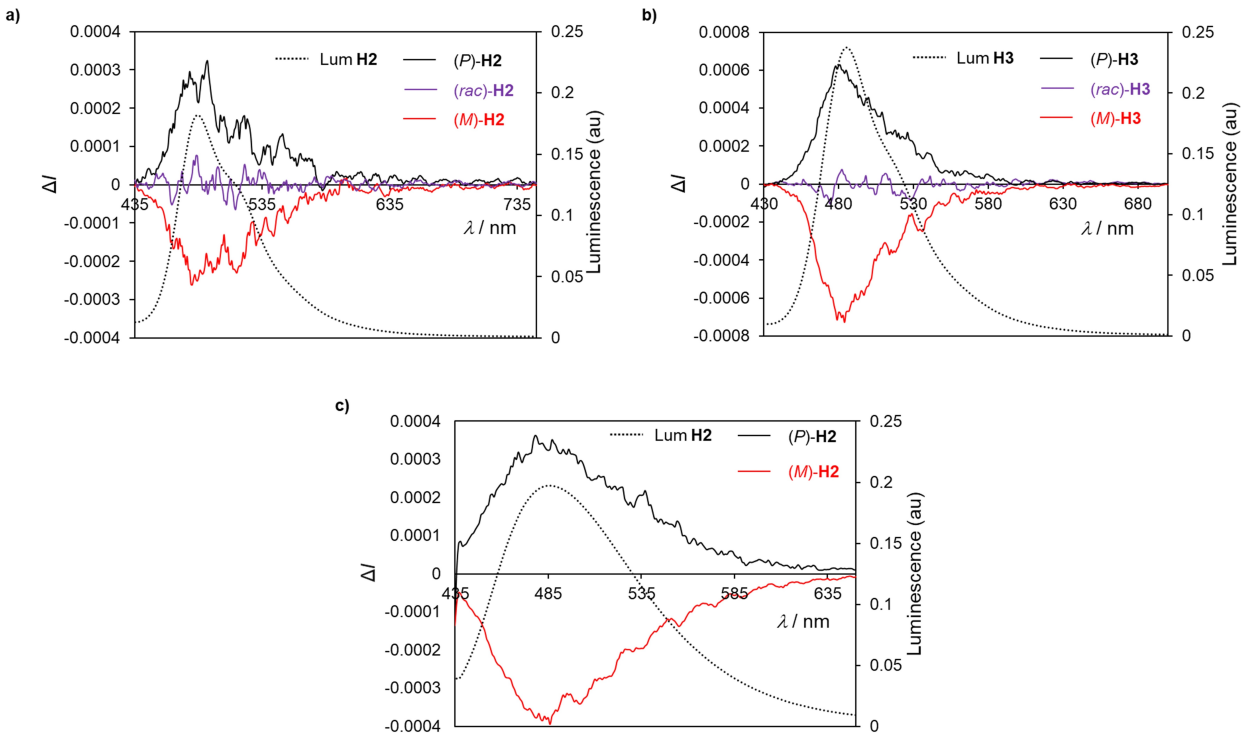

Figure 5. Experimental emission and CPL spectra of (*P*) and (*M*) enantiomers of a) **H2** and b) **H3** in CH_2Cl_2 at $C \sim 10^{-5}$ M and rt, and c) **H2** in PMMA. Excitation wavelengths are 390 and 385 nm for **H2** and **H3**, respectively.

CH_2Cl_2). The computations involving S_1 excited-state geometry optimizations reproduced correctly experimental energetic positions of the emission maxima and their overall slight red-shift when going from **H1** to **H2** to **H3** and confirmed that in each case $S_1 \rightarrow S_0$ fluorescence transition is of the boranil-centered π–π^* character with some helicene→boranil CT signature (see Table S2.5 and Figure S2.15). Overall small CT component in the emission is in line with the aforementioned, rather minor effect of a solvent polarity on the experimentally observed fluorescence spectra of these compounds.

Circularly polarized luminescence

Helicenes are known to exhibit efficient circularly polarized fluorescence or phosphorescence activity, which makes them appealing for incorporation into OLEDs as circularly polarized electroluminescent materials.[2] The CPL spectra of (*P*) and (*M*) enantiomers of **H2** and **H3** derivatives and of their racemic samples were thus recorded in CH_2Cl_2 at rt. As expected, the enantiomers revealed mirror-image CPL relationships, while the racemic samples exhibited no CPL activity. Regarding the dissymmetry factors, which reflect the percentage of circularly polarized emitted light ($g_{lum} = 2(I_L - I_R)/(I_L + I_R)$), we obtained g_{lum} of $-1.3\times10^{-3}/+1.2\times10^{-3}$ for **H2** and $-2.5\times10^{-3}/+2.5\times10^{-3}$ for **H3**, for (*M*)/(*P*) enantiomers, respectively. The fact that **H3** displays higher g_{lum} values compared to **H2** is in agreement with our previous results on helicene-diketopyrrolopyrrole and -naphthalimide derivatives.[21] In particular, a clear reminiscence to the former systems can be noted here, with the bis-boranil derivative **H3** showing exciton coupling chirality based on a typical low-energy substituent-centered excition couplet which induces enhanced chiroptical activity and stronger CPL (*vide supra*). The calculations correctly reproduced an increase (roughly doubling) of the g_{lum} values for **H3** *vs.* **H2** and linked it predominantly to an increase in rotatory strength of $S_1 \rightarrow S_0$ fluorescence transition for the bis-boranil system. The analysis showed that this enhancement can be in turn traced back to a more beneficial orientation (an increased deviation of the angle from 90°) between the underlying electric and magnetic transition dipole moments observed for **H3** as compared to **H2** (see Table S2.6 and Figure S2.16). This might indeed be a reflection of the exciton coupling effect in the excited state of **H3** with the resulting lower-energy couplet's component representing the S_1 state being the emitting one. Finally, it was appealing to see whether these derivatives display CPL activity in the solid state. Indeed, spin-coated films of (*P*)- and (*M*)-**H2** (0.2% in weight in PMMA films) gave nice mirror-image CPL signals with maximum emission at 490 nm and g_{lum} values similar to the solution state (Figure 5c), *i.e.* around $\pm10^{-3}$. Satisfyingly, these chiral films appeared fully isotropic (see Supporting Information).

Conclusion

We have prepared a new family of boron-substituted helicene derivatives that enriches both helicenes and boranils chemistry, namely carbo[4]helicene-2-mono-boranil (**H1**) along with carbo [6]helicene-2-mono- and -2,15-bis-boranils (**H2** and **H3**, respectively), which display fluorescence emission in solution. Furthermore, enantiopure **H2** and **H3** systems also show efficient circularly polarized luminescence, with absolute g_{lum} values up to 2.5×10^{-3} demonstrated by the bis-boranil derivative thanks to the exciton coupling effect. The X-ray structure analysis of **H2** revealed an interesting chiral induction from the helicenic part to the axial chirality that arises due to the presence of a CH-π interaction between a proton of the boranil unit and the carbo[6]helicene core which 'locks' the structure into a closed form of energetically preferred (P,R_a)/(M,S_a) stereochemistry in the solid state. As a result, the system keeps its CPL activity in PMMA films. In the solution, coexistence of various structures of both (R_a) and (S_a) axial chirality is however expected based on both experimental and computational results. These structural aspects put forward novel features in the domain of helicenes and might inspire further research aiming at preserving and controlling specific axially chiral conformations also in solution.

Acknowledgements

We acknowledge the Centre National de la Recherche Scientifique (CNRS) and the University of Rennes. This work was supported by the Agence Nationale de la Recherche (ANR-16-CE07-0019 "Hel-NHC" grant). M.S.-H. thanks the PL-Grid Infrastructure and the ACC Cyfronet AGH in Krakow, Poland for providing computational resources. Dr. Ludovic Favereau is warmly thanked for fruitful discussions.

Conflict of Interest

The authors declare no conflict of interest.

Keywords: boranil · chirality · circularly polarized luminescence · helicene · quantum chemistry

[1] a) Y. Shen, C.-F. Chen, *Chem. Rev.* **2012**, *112*, 1463–1535; b) M. Gingras, *Chem. Soc. Rev.* **2013**, *42*, 1051–1095; c) Y. Shen, C.-F. Chen, *Helicenes Chemistry: From Synthesis to Applications*, Springer, Berlin, **2017**.

[2] a) W.-L. Zhao, M. Li, H.-Y. Lu, C.-F. Chen, *Chem. Commun.* **2019**, *55*, 13793–13803; b) J. Crassous in *Circularly Polarized Luminescence of Isolated Small Organic Molecules*, (Ed.: T. Mori), Springer, **2020**, chap. 4, pp 53–97.

[3] a) F. S. Richardson, J. P. Riehl, *Chem. Rev.* **1977**, *77*, 773–792; b) J. P. Riehl, F. S. Richardson, *Chem. Rev.* **1986**, *86*, 1–16; c) J. Kumar, T. Nakashima, T. Kawai, *J. Phys. Chem. Lett.* **2015**, *6*, 3445–3452; d) B. Kunnen, C. Macdonald, A. Doronin, S. Jacques, M. Eccles, I. Meglinski, *J. Biophotonics* **2015**, *8*, 317–323; e) E. M. Sánchez-Carnerero, A. R. Agarrabeitia, F. Moreno, B. L. Maroto, G. Muller, M. J. Ortiz, S. de la Moya, *Chem. Eur. J.* **2015**, *21*, 13488–13500; f) J. Han, S. Guo, H. Lu, S. Liu, Q. Zhao, W. Huang, *Adv. Opt. Mater.* **2018**, *6*, 1800538.

[4] a) F. Zinna, L. Di Bari, *Chirality* **2015**, *27*, 1–13; b) R. Carr, N. H. Evans, D. Parker, *Chem. Soc. Rev.* **2012**, *41*, 7673–7686; c) G. Muller, *Dalton Trans.* **2009**, 9692–9707.
[5] Selected examples: a) L. Norel, M. Rudolph, N. Vanthuyne, J. A. G. Williams, C. Lescop, C. Roussel, J. Autschbach, J. Crassous, R. Réau, *Angew. Chem. Int. Ed.* **2010**, *49*, 99–102; *Angew. Chem.* **2010**, *122*, 103–106; b) K. Nakamura, S. Furumi, M. Takeuchi, T. Shibuya, K. Tanaka, *J. Am. Chem. Soc.* **2014**, *136*, 5555–5558; c) K. Murayama, Y. Oike, S. Furumi, M. Takeuchi, K. Noguchi, K. Tanaka, *Eur. J. Org. Chem.* **2015**, 1409–1414; d) C. Schaack, L. Arrico, E. Sidler, M. Górecki, L. Di Bari, F. Diederich, *Chem. Eur. J.* **2019**, *25*, 8003–8007.
[6] K. Dhbaibi, L. Favereau, J. Crassous, *Chem. Rev.* **2019**, *119*, 8846–8953.
[7] a) C. Shen, M. Srebro-Hooper, M. Jean, N. Vanthuyne, L. Toupet, J. A. G. Williams, A. R. Torres, A. J. Riives, G. Muller, J. Autschbach, J. Crassous, *Chem. Eur. J.* **2017**, *23*, 407–418. For longer analogues see:; b) J. Full, S. P. Panchal, J. Götz, A.-M. Krause, A. Nowak-Król, *Angew. Chem.* **2021**, *60*, 4350–4357; *Angew. Chem.* **2021**, *133*, 4396–4403.
[8] Z. Domínguez, R. López-Rodríguez, E. Álvarez, S. Abbate, G. Longhi, U. Pischel, A. Ros, *Chem. Eur. J.* **2018**, *24*, 12660–12668.
[9] T. Katayama, S. Nakatsuka, H. Hirai, N. Yasuda, J. Kumar, T. Kawai, T. Hatakeyama, *J. Am. Chem. Soc.* **2016**, *138*, 5210–5213.
[10] a) C. Maeda, K. Nagahata, T. Shirakawa, T. Ema, *Angew. Chem. Int. Ed.* **2020**, *59*, 7813–7817; *Angew. Chem.* **2020**, *132*, 7887–7891; b) E. M. Sánchez-Carnerero, F. Moreno, B. L. Maroto, A. R. Agarrabeitia, M. J. Ortiz, B. G. Vo, G. Muller, S. de la Moya, *J. Am. Chem. Soc.* **2014**, 136, 3346–3349.
[11] P. M. Lorente, A. Wallabregue, F. Zinna, C. Besnard, L. Di Bari, J. Lacour, *Org. Biomol. Chem.* **2020**, *18*, 7677–7684.
[12] Z.-H. Zhao, X. Liang, M.-X. He, M.-Y. Zhang, C.-H. Zhao, *Org. Lett.* **2019**, 21, 9569–9573.
[13] For recent examples, see: a) R. P. Nandi, P. Sudhakar, N. K. Kalluvettukuzhy, P. Thilagar, *Chem. Eur. J.* **2020**, *26*, 16306–16317; b) S. Agren, M. Chaabene, A.-R. Allouche, R. Ben Chaabane, M. Lahcinie, M. H. V. Baouab, *Appl. Organomet. Chem.* **2020**, *34*, e5764; c) A. Ren, D. Zhu, Y. Luo, *J. Mol. Struct.* **2020**, *1209*, 127914; d) H. H. T. Al-Sharif, R. Ziessel, P. G. Waddell, C. Dixon, A. Harriman, *J. Phys. Chem. A* **2020**, *124*, 2160–2172; e) N. Zhao, C. Ma, W. Yang, W. Yin, J. Wei, N. Li, *Chem. Commun.* **2019**, *55*, 8494–8497; f) D. Zhu, X. Yan, A. Ren, W. Cai, Z. Duan, Y. Luo, *Anal. Methods* **2019**, *11*, 2579–2584.
[14] F. Umland, E. Hohaus, K. Brodte, *Chem. Ber.* **1973**, *106*, 2427–2437.
[15] D. Frath, S. Azizi, G. Ulrich, P. Retailleau, R. Ziessel, *Org. Lett.* **2011**, *13*, 3414–3417.
[16] a) P. A. A. M. Vaz, J. Rocha, A. M. S. Silva, S. Guieu, *New J. Chem.* **2018**, *42*, 18166–18171; b) Y. Zhou, J. W. Kim, M. J. Kim, W.-J. Son, S. J. Han, H. N. Kim, S. Han, Y. Kim, C. Lee, S.-J. Kim, D. H. Kim, J.-J. Kim, J. Yoon, *Org. Lett.* **2010**, *12*, 1272–1275; c) Z. Jiang, X. Wang, J. Ma, Z. Liu, *Sci. China Chem.* **2019**, *62*, 355–362.
[17] a) V. G. Jiménez, F. M. F. Santos, S. Castro-Fernández, J. M. Cuerva, P. M. P. Gois, U. Pischel, A. G. Campaña, *J. Org. Chem.* **2018**, *83*, 14057–14062; b) J. Li, X. Peng, C. Huang, Q. Qi, W.-Y. Lai, W. Huang, *Polym. Chem.* **2018**, *9*, 5278–5285.
[18] a) A. Macé, N. Hellou, J. Hammoud, C. Martin, E. S. Gauthier, L. Favereau, T. Roisnel, E. Caytan, G. Nasser, N. Vanthuyne, J. A. G. Williams, F. Berrée, B. Carboni, J. Crassous, *Helv. Chim. Acta* **2019**, *102*, e1900044; b) N. Hellou, A. Macé, C. Martin, V. Dorcet, T. Roisnel, M. Jean, N. Vanthuyne, F. Berrée, B. Carboni, J. Crassous, *J. Org. Chem.* **2018**, *83*, 484–490.
[19] a) A. Terfort, H. Gorls, H. Brunner, *Synthesis* **1997**, *1*, 79–86; b) C. Shen, F. Gan, G. Zhang, Y. Ding, J. Wang, R. Wang, J. Crassous, H. Qiu, *Mater. Chem. Front.* **2020**, *4*, 837–844.
[20] X. Xie, Y. Yuan, R. Krüger, M. Bröring, *Magn. Reson. Chem.* **2009**, *47*, 1024–1030.
[21] a) K. Dhbaibi, L. Favereau, M. Srebro-Hooper, M. Jean, N. Vanthuyne, F. Zinna, B. Jamoussi, L. Di Bari, J. Autschbach, J. Crassous, *Chem. Sci.* **2018**, *9*, 735–742; b) K. Dhbaibi, L. Favereau, M. Srebro-Hooper, C. Quinton, N. Vanthuyne, L. Arrico, T. Roisnel, B. Jamoussi, C. Poriel, C. Cabanetos, J. Autschbach, J. Crassous, *Chem. Sci.* **2020**, *11*, 567–576.
[22] a) M. Srebro-Hooper, J. Autschbach, *Annu. Rev. Phys. Chem.* **2017**, *68*, 399–420; b) J. Autschbach, *Chirality* **2009**, *21*, E116-E152.
[23] a) O. E. Weigang Jr., J. A. Turner, P. A. Trouard, *J. Chem. Phys.* **1966**, *45*, 1126–1134; b) Y. Liu, J. Cerezo, G. Mazzeo, N. Lin, X. Zhao, G. Longhi, S. Abbate, F. Santoro, *J. Chem. Theory Comput.* **2016**, *12*, 2799–2819; c) Q. Xu, Y. Liu, X. Zhao, S. Chen, Q. Li, M. Wang, C. Yang, *Spectrochim. Acta Part A* **2020**, *231*, 118132; d) Y. Liu, Q. Xu, J. Sun, L. Wang, D. He, M. Wang, C. Yang, *Spectrochim. Acta Part A* **2020**, *239*, 118475.
[24] C. Bannwarth, J. Seibert, S. Grimme, *Chirality* **2016**, *28*, 365–369.
[25] M. El Sayed Moussa, M. Srebro, E. Anger, N. Vanthuyne, C. Roussel, C. Lescop, J. Autschbach, J. Crassous, *Chirality* **2013**, *25*, 455–465.
[26] N. Zhao, C. Ma, W. Yang, W. Yin, J. Wei, N. Li, *Chem. Commun.* **2019**, *55*, 8494–8497.

Manuscript received: January 29, 2021
Accepted manuscript online: March 26, 2021
Version of record online: ■■, ■■■

FULL PAPER

Helicene-mono- and bis-boranils have been prepared in enantiopure forms. The chiroptical (electronic circular dichroism and optical rotation) and photophysical properties (unpolarized and circularly polarized luminescence) of these new chiral emissive helicenes have been studied both experimentally and theoretically and highlight their combined helical and axial chirality effects.

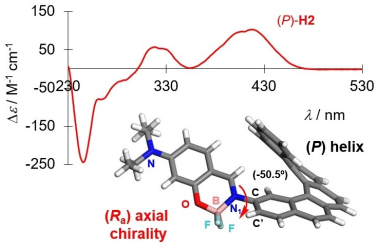

Dr. A. Macé, K. Hamrouni, Dr. E. S. Gauthier, M. Jean, Dr. N. Vanthuyne, Dr. L. Frédéric, Dr. G. Pieters, Dr. E. Caytan, Dr. T. Roisnel, Dr. F. Aloui, Dr. M. Srebro-Hooper, Dr. B. Carboni, Dr. F. Berrée*, Dr. J. Crassous**